J Mater Sci (2014) 49:5112–5118
DOI 10.1007/s10853-014-8220-5

The effect of the coupling agents KH550 and KH570 on the nanostructure and interfacial interaction of zinc oxide/chiral poly(amide–imide) nanocomposites containing L-leucine amino acid moieties

Shadpour Mallakpour · Maryam Madani

Received: 15 February 2014 / Accepted: 3 April 2014 / Published online: 22 April 2014

Abstract In this article, a series of optically active poly(amide–imide)/zinc oxide nanocomposites (PAI/ZnO NCs) with different ZnO contents were prepared by ultrasonic technique. For better dispersion of nanoparticles (NPs) in the PAI matrix, their surface was modified with two different silane coupling agents. Then, the effects of two linkers on dispersity of NPs, thermal stability and UV–Visible spectra of resulting NCs were investigated. The morphological structures, thermal, and UV properties of the prepared NCs with two different coupling agents were studied by X-ray diffraction, transmission electron micrograph, field emission scanning electron microscopy, thermogravimetric analysis, and UV–Visible analysis. These data demonstrated that the surface-modified ZnO NPs were homogeneously dispersed in the PAI matrix. However, in the case of KH570 the better dispersity is more pronounced.

Introduction

An intensive range of research has been devoted to developing polymer properties using nanotechnology. These new materials are known as nanocomposites (NCs), which are multiphase solids where one of the phases has at least one dimension in the nanometer scale. These materials including polymers, metal nanoparticles (NPs), and metal oxide NPs have excellent properties of individual components and reinforcing each other's properties simultaneously because the interfacial interaction between the filler and the polymer is strong [1–3].

Semiconductor NPs have attracted much attention due to their novel optical, electrical, and mechanical properties. Among various semiconductor NPs, zinc oxide (ZnO) NPs have attracted significant attention due to their proposed applications in solar energy conversion [4], varistors [5], luminescence [6], photocatalysis [7, 8], coating [9], and chemical sensors [10, 11].

The control of dispersion homogeneity of the NPs over the polymer is important. Therefore, the surface of NPs was modifying with coupling agents. Trialkoxysilane of coupling agent molecules hydrolyzes in solution and finally condense with hydroxyl groups at the surface of NPs [12–14].

Aromatic poly(amide–imide)s (PAIs) have been developed as high-performance materials offering a good compromise between thermal stability and processability. Comparing with the polyimide and polyamide, the PAI own the better process ability and heat resistant properties [15–17]. Therefore, it is suitable matrix for the preparation of NC [18–21]. Consequently, a wide range of aromatic PAIs have been used for wire-coating enamels, adhesives, composite materials, fiber, and film material. On the other hand, to achieve biodegradation properties using multifunctional natural metabolites such as amino acids may be useful. These materials are naturally occurring compounds; so, polymers based on amino acids are expected to be biodegradable and biocompatible. Recently, Mallakpour and co-workers reported synthesis and application of different kinds of optically active polymers [22–25].

S. Mallakpour (✉) · M. Madani
Organic Polymer Chemistry Research Laboratory, Department of Chemistry, Isfahan University of Technology, Isfahan 84156-83111, Islamic Republic of Iran
e-mail: mallak@cc.iut.ac.ir; mallak777@yahoo.com; mallakpour84@alumni.ufl.edu

S. Mallakpour
Nanotechnology and Advanced Materials Institute, Isfahan University of Technology, Isfahan 84156-83111, Islamic Republic of Iran

In this study, PAI/ZnO-based hybrid materials, without extensive chemical bonding between two phases has been explored using ultrasonication process. For preparation of PAI, which used as matrix of NCs, at first, optically active diacid, *N*-trimellitylimido-L-leucine was prepared. Then, the PAI was synthesized by direct polycondensation reaction of this diacid with 4,4′-diaminodiphenylether, in the tetrabutylammonium bromide/triphenyl phosphite (TBAB/TPP) as condensing agent and green reaction media. The interaction between organic and inorganic phases was performed using two different linkers, γ-methacryloxypropyltrimethoxy silane (KH570) and γ-aminopropyltriethoxy silane (KH550) as coupling agents. The properties of resulting NCs from each coupling agent were studied comparatively by X-ray diffraction (XRD), field emission scanning electron microscopy (FE-SEM), and transmission electron micrograph (TEM). The thermal and optical properties investigated by thermogravimetric analysis (TGA), and UV–Visible analysis (UV–Vis).

Experimental

Materials

All chemicals were purchased from Fluka Chemical Co. (Buchs, Switzerland), Aldrich Chemical Co. (Milwaukee, WI, USA), Riedel-deHaen AG (Seelze, Germany), and Merck Chemical Co. (Darmstadt, Germany). L-leucine ($C_6H_{13}NO_2$, 131.17 g mol^{-1}, ≥99 %) and 4,4′-diaminodiphenylethre were used as obtained without further purification. The silane coupling agents, KH570 and KH550 obtained from Merck Chemical Co. Nanosized ZnO powder was purchased from Neutrino Co.(Tehran, Iran) with average particle sizes of 25–30 nm.

Equipments

A Jasco-680 Fourier transform infrared (FT-IR) spectrophotometer (Japan) was employed to examine the chemical bonds on the polymer and NCs. Spectra of solids were obtained with KBr pellets. Inherent viscosities were measured by a standard procedure using a Cannon–Fenske routine viscometer (Germany) at the concentration of 0.5 g/dL at 25 °C. Specific rotations were measured by a Jasco Polarimeter (Japan). TGA is performed with a STA503 win TA at a heating rate of 10 °C/min from 25 to 800 °C under nitrogen. The XRD pattern was acquired by using a Philips Xpert MPD X-ray diffractometer. The diffractograms were measured for 2θ, in the range of 10–100°, using Cu K_α incident beam (λ = 1.51418 Å). FE-SEM micrographs of samples were taken on a Hitachi (S-4160). The morphology and dispersity analysis was performed on TEM analyzer on Philips CM 120 operating at 100 kV. UV–Vis absorption of PAI/ZnO NCs were measured on a UV–Vis spectrometer JASCO V-750 in the spectral range between 200 and 800 nm. A horn probe MISONIX ultrasonic liquid processor, XL-2000 SERIES with frequency 2.25 × 10^4 Hz and power 100 W was used in solution mixture.

Polymer synthesis

N-trimellitylimido-L-leucine (**3**) was prepared by the condensation of L-leucine (**2**) with trimellitic anhydride (**1**), according to the previously reported procedure [26]. A typical preparation of PAI is as follows: into a dried 25 mL round-bottomed flask equipped with a water-cooled condenser and a magnetic stirrer, 0.30 g (0.98 mmol) diacid (**3**), 0.19 g (0.98 mmol) 4,4′-diaminodiphenyl ether (**4**) and 1.26 g (3.92 mmol) TBAB was ground then 0.93 mL (3.92 mmol; density = 1.1 g/cm^3) TPP was added. The temperature of mixture was raised to 120 °C and held for 12 h. The resulting product was isolated by addition of 30 mL of methanol. Powdered polymer was dried to leave 0.45 g (90 %) of PAI (Scheme 1). The inherent viscosity and optical rotation of this PAI in dimethylformamide (DMF) (measured at a concentration of 0.5 g dL^{-1} at 25 °C) was 0.20 dL g^{-1} and −18.86°, respectively.

Preparation of PAI/ZnO NCs

Initially, the ZnO NPs modified with silane coupling agent. Two different coupling agents (KH570 and KH550) were

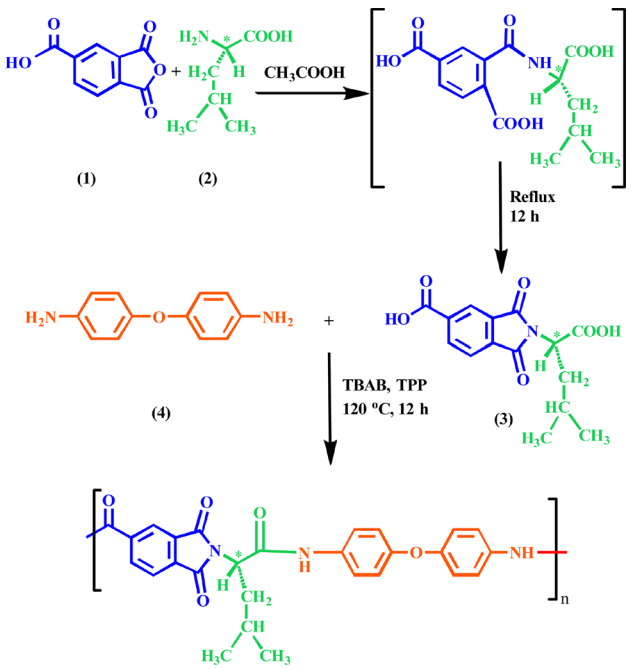

Scheme 1 Synthesis of monomer (**3**) and preparation of PAI

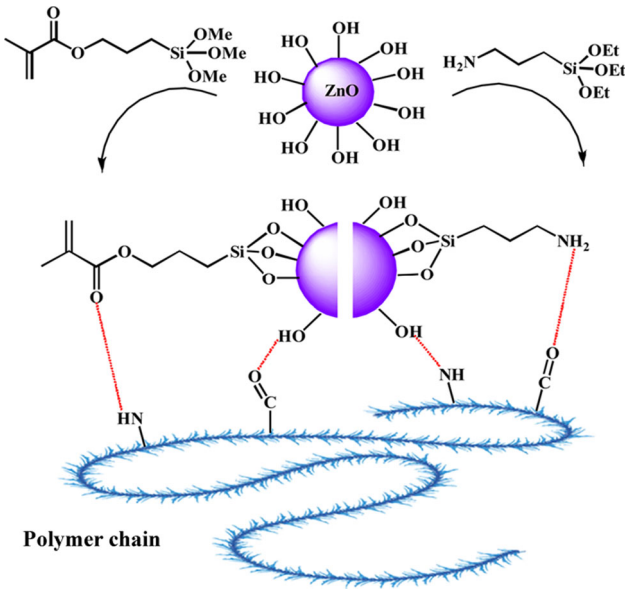

Scheme 2 Reaction of ZnO NPs with two different coupling agents and preparation of PAI/ZnO NC

investigated to improve the properties of the interphase. The ZnO was dried at 110 °C for 24 h before the surface modification. Then, 0.20 g dried nano ZnO was ultrasonicated for 15 min in ethanol (20 wt % ZnO) and KH550 or KH570 coupling agent was added to system and ultrasonicated for 20 min; at last, the mixture was filtered and dried at 60 °C for more than 24 h.

For preparation of NC, PAI scattered in 20 mL of ethanol then different amounts of modified ZnO NPs (4, 8, and 12 wt %) were mixed with suspension and irradiated under ultrasound waves for 4 h. The solvent removed and the obtained solid dried in vacuum at 80 °C for 4 h (Scheme 2).

Results and discussion

Fabrication of PAI/ZnO NCs

PAI/ZnO NCs were prepared by an ultrasonic irradiation technique. In process of modification of NPs, the hydroxyl group on the surface of ZnO will be replaced with alkoxyl substituents of the silane groups. Silanol group, which is linked on the surface of ZnO, will produce steric repulsion that can prevent their aggregation. The modification illustration of ZnO NPs with KH570 and KH550 is shown in Scheme 2. The modified NPs will combine with PAI via the H-bonding (C=O group of KH570 coupling agent and $–NH_2$ group of KH550 coupling agent with –NH, C=O groups in PAI). The unmodified –OH groups on the surface of NPs can bond to C=O and –NH of PAI through hydrogen bonding. The details of proposed interactions in PAI NCs are displayed in Scheme 2.

FT-IR spectra

Figure 1 shows typical the FT-IR spectra of pure ZnO NPs and ZnO NPs modified with coupling agents (KH570 and KH550). The FT-IR spectrum of ZnO NPs showed the broad peak at 3434 cm^{-1} due to the stretching vibrations of the –OH group on the surface of ZnO NPs, a high intensity broad band around 424 cm^{-1} is owing to the stretching mode of the Zn–O bond. The spectrum of ZnO NPs modified with the KH570 coupling agent showed the absorption peaks at 2929 ($–CH_2$), 1718 (C=O), 1636 (C=C), 1170 (SiOH), 939 (Zn–O–Si), 817 (Si–O-Si) cm^{-1}, which were characteristic peaks of functional groups of linker and indicating that KH570 was bonded to the surface of nano ZnO.

The FT-IR spectrum of functionalized ZnO with KH550 gave a broad absorption band located at 3419 cm^{-1}, which attributed to –OH and $–NH_2$. The peaks at 2928 and 1016 cm^{-1} can be assigned to the symmetric methylene stretch ($–CH_2$), and the Si–O stretch, respectively. The FT-IR indicated that coupling agents were successfully grafted onto the surface of ZnO NPs.

The FT-IR spectra of the PAI and NCs containing 12 wt % of modified ZnO NPs with coupling agents are shown in Fig. 2. The spectrum of pure PAI showed absorptions around 3324 cm^{-1} (N–H), and two overlapped carbonyl (amide and imide's C=O) absorptions at 1776, 1719, and 1669 cm^{-1}, respectively. The peaks at 1378 and 727 cm^{-1} indicate the presence of the imide heterocycle in this polymer structure. The spectra of the NCs with both coupling agents display the characteristic absorption peaks matching to polymeric groups. The peaks at the region from 400 to 800 cm^{-1} assigned to Zn–O still existed.

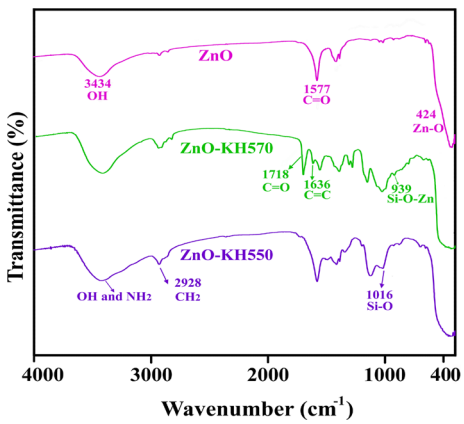

Fig. 1 FT-IR spectra of ZnO NPs, ZnO–KH570, and ZnO–KH550 NPs

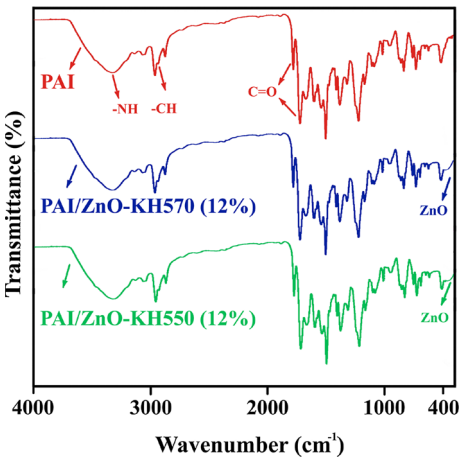

Fig. 2 FT-IR spectra of PAI, PAI/ZnO–KH570 (12 wt %) and PAI/ZnO–KH550 (12 wt %)

X-ray diffraction

The XRD patterns of ZnO, PAI/ZnO–KH570 (12 wt %), PAI/ZnO–KH550 (12 wt %), and PAI are shown in Fig. 3. Pure PAI did not show any sharp diffraction peaks and is more or less amorphous. Figure 3b and c shows the XRD pattern of NCs with 12 wt % of ZnO NPs with KH570 and KH550 coupling agent, respectively, indicating the morphology of ZnO NPs has not been distorted during the sonication. In Fig. 3d, a series of characteristic peaks: (100), (002), (101), (102), (110), (103), (200), (112), and (201) are noticed, which are related to the zincite phase of ZnO (International Center for diffraction data, JCPDS 5-0664). The average crystallite size D was calculated by the Debye–Scherrer formula $(D = K\lambda/\beta\cos\theta)$, where K is the Scherrer constant, λ is the X-ray wavelength, β is the peak width at half-maximum, and θ is the Bragg diffraction angle. From the Debye–Scherrer formula, we obtained the crystallite diameter as 25–38 nm for ZnO–KH570 and 23–40 nm for ZnO–KH550 in polymer matrix.

Morphology studies

Figure 4 shows the fractal surface of PAI, PAI/ZnO–KH570 12 wt %, and PAI/ZnO–KH550 12 wt % NC. From FE-SEM images, it was found that the functionalized ZnO with two different linkers were quasi-spherical in shape. The results showed that ZnO NPs were homogeneously dispersed in PAI matrix and their average particle size was below 70 nm. However, the dispersion of NPs in the PAI matrix was different from one coupling agent to another. It is interesting to mention that the size of NPs with KH550 coupling agent is bigger than of KH570 and shows a little aggregation.

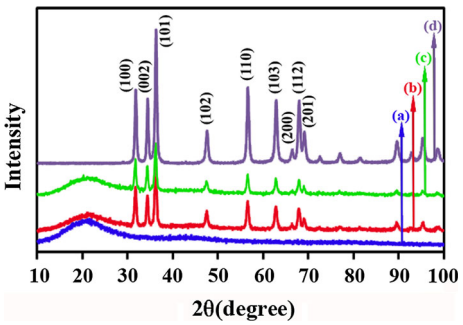

Fig. 3 XRD patterns of (a) PAI, (b) PAI/ZnO–KH570 (12 wt %), (c) PAI/ZnO–KH550 (12 wt %), and (d) ZnO

Figure 5 shows the representative TEM micrograph of PAI/ZnO NC. Figure 5a and b shows the morphology of PAI/ZnO–KH570 (12 wt %) NC. The micrographs confirmed that dispersing ZnO–KH570 particles in the polymer matrix is rather good and the size of NPs are ranging from 30 to 50 nm. The morphological images of the PAI/ZnO–KH550 (12 wt %) shown in Fig. 5c and d. From these photographs, it is obvious that the particles size is rather large and some agglomerations of them are observable. The FE-SEM and TEM results show that, when ZnO is treated with coupling agents, the dispersion of NPs in polymer matrix is improved obviously. In other words, the interfacial interaction is very important to improve the NC properties. NPs due to large specific surface area and high surface energy can cause agglomeration of particles in the polymer matrix. Consequently, modification of ZnO NPs is necessary. TEM image indicated that the coupling agents behavior play an important role in dispersing the NPs. In this investigation, it was found that KH570 linker with functional group of methacrylate is more efficient than KH550 in improving the NPs dispersion. For coupling agent KH550, functional group that provides the interaction to the PAI matrix is the amino group. The NH_2 of side group in KH550 may interact with each other before connected to ZnO particles or may form double layer.

Thermal analysis

Figure 6 shows the TGA curves of PAI/ZnO–KH570 NC with different content of the modified ZnO NPs. The samples display a good thermal stability before 300 °C, which was further improved when modified ZnO NPs was introduced. The char yields at 800 °C of the NCs with different ZnO content are higher than that of the pure PAI. This increase in thermal stability may result from the high thermal stability of the ZnO NPs. Thermal behavior of PAI/ZnO–KH550 shows in Fig. 7. According to the results of TGA data in Table 1, the thermal stability of PAI with the KH570 linker is higher than the KH550. Therefore, nature

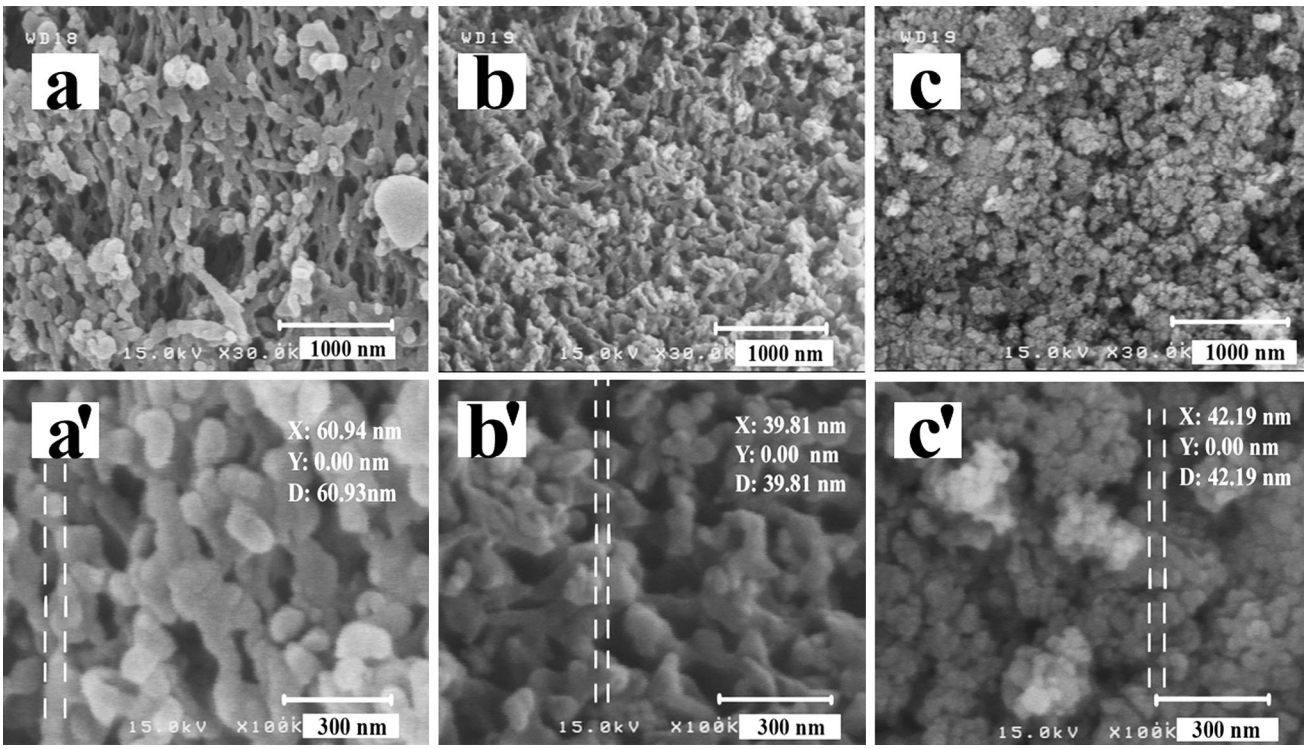

Fig. 4 FE-SEM micrographs of pure PAI (**a**, **a**′), PAI/ZnO–KH570 (12 wt %) (**b**, **b**′), and PAI/ZnO–KH550 (12 wt %) (**c**, **c**′) with different magnification

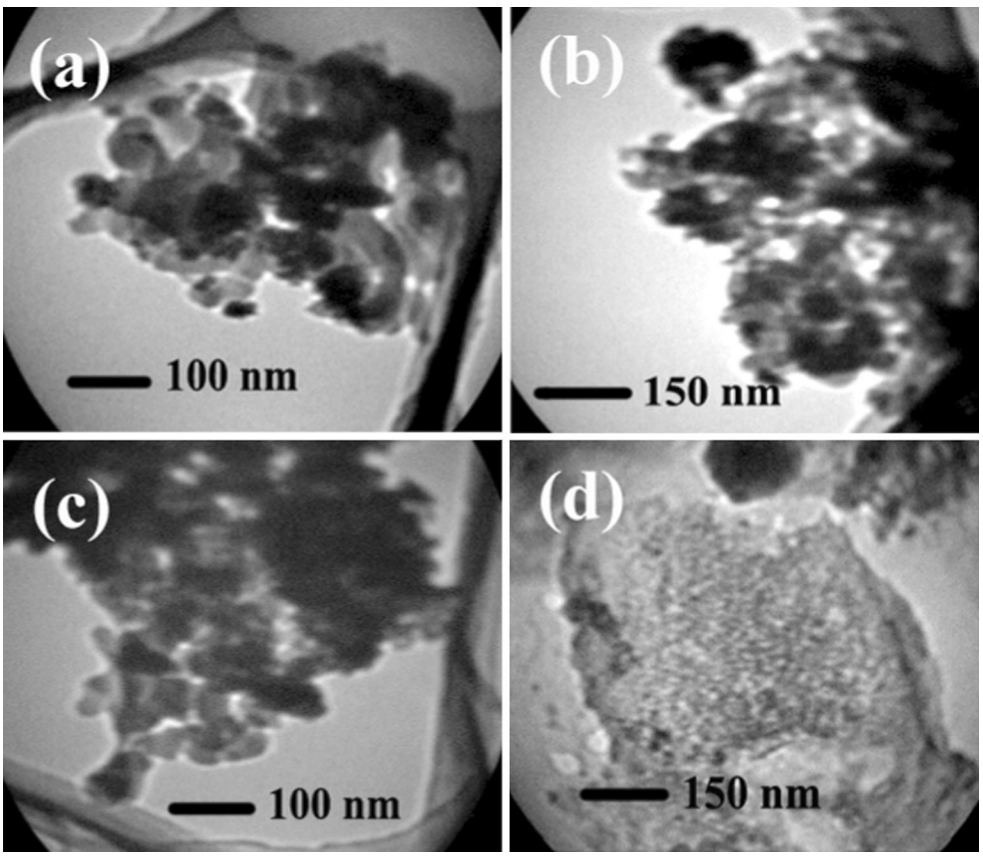

Fig. 5 TEM micrograph of **a**, **b** PAI/ZnO–KH570 (12 wt %) and **c**, **d** PAI/ZnO–KH550 (12 wt %) with different magnification

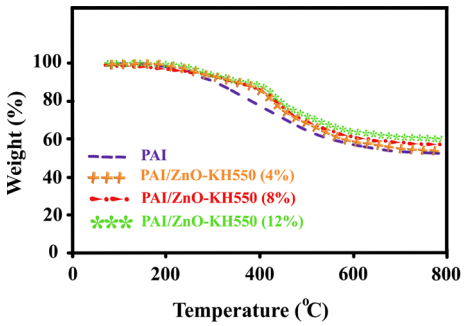

Fig. 6 TGA thermograms of PAI and PAI/ZnO–KH570 nanocomposites with different nanofiller content

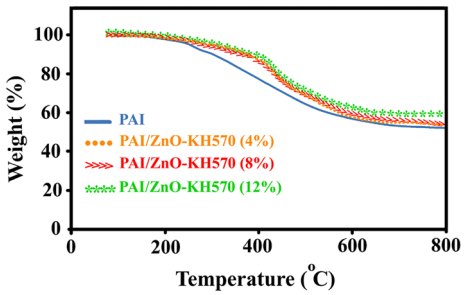

Fig. 7 TGA thermograms of PAI and PAI/ZnO–KH550 nanocomposites with different nanofiller content

Table 1 Thermal properties of the PAI and PAI/ZnO bionanocomposites

Polymer	T_5 (°C)[a]	T_{10} (°C)[b]	Char yield (%)[c]
Pure PAI	255.0	304.7	52.2
PAI/ZnO–KH550 (4 wt %)	270.0	340.0	54.0
PAI/ZnO–KH570 (4 wt %)	286.0	369.0	53.0
PAI/ZnO–KH550 (8 wt %)	271.0	343.0	56.5
PAI/ZnO–KH570 (8 wt %)	286.0	364.0	56.6
PAI/ZnO–KH550 (12 wt %)	275.0	350.0	60.0
PAI/ZnO–KH570 (12 wt %)	293.0	375.0	60.0

[a] Temperature at which 5 % weight loss was recorded by TGA at heating rate of 10 °C/min under a nitrogen atmosphere

[b] Temperature at which 10 % weight loss was recorded by TGA at heating rate of 10 °C/min under a nitrogen atmosphere

[c] Weight percentage of material left undecomposed after TGA analysis at a temperature of 800 °C under a nitrogen atmosphere

of coupling agent effects on thermal stability of the obtained NCs. In result, the more hydrogen bonding, the higher thermal stability is expected. Since ZnO–KH570 makes more hydrogen bonding with the polymer matrix, than the ZnO–KH550, hence, the thermal stability of the PAI/ZnO NCs derived from ZnO–KH570 is higher. This can be simply recognized from the Figs. 6 and 7.

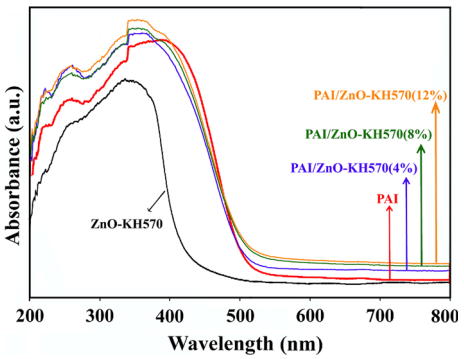

Fig. 8 UV/Vis absorption spectra of ZnO–KH570, PAI, and PAI/ZnO nanocomposites

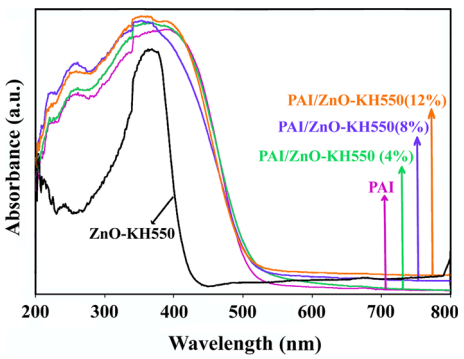

Fig. 9 UV/Vis absorption spectra of ZnO–KH550, PAI, and PAI/ZnO nanocomposites

UV–Vis absorption

The UV–Vis absorbance spectra of PAI and PAI/ZnO NCs are shown in Figs. 8 and 9. The maximum absorption peak of pure PAI is shown at near 386 nm due to its delocalized π electrons. The surface-modified ZnO NPs show a maximum UV absorption peak at 338 and 368 nm for KH570 and KH550 coupling agent, respectively. For the PAI/ZnO NCs with two different coupling agents, the maximum absorption peak of polymer is shifted to the maximum absorption peak of the modified ZnO NPs. The obtained NCs have UV shielding ability, hence it is expected that these NCs can be applied to block the UV radiation.

Conclusions

Modified ZnO/PAI NCs were prepared by ultrasonic irradiation. Nanostructure ZnO was modified with two linkers (KH570 and KH550) and their effects on the properties of the obtained ZnO/PAI NCs were compared. The NCs performance and morphologies are remarkably influenced by dispersing aid and type of coupling agent. The results

suggested that the kind of coupling agent was an effective treatment to increase the thermal stability of the NCs. The TGA data showed that thermal stability of NCs reinforced with ZnO–KH570 is higher than ZnO–KH550. Therefore, depending on the nature of coupling agent, compatibility of ZnO NPs with PAI matrix increased and the dispersion of NPs were improved. The morphological behaviors of NCs were investigated by FE-SEM and TEM and the results showed that the modification of ZnO NPs with KH570 coupling agent was more effective than KH550. Optical properties characterization results indicated that the NCs have absorption around the UV region so it is anticipated that these materials can be used as UV shielding materials.

Acknowledgements We gratefully acknowledge the partial financial support from the Research Affairs Division Isfahan University of Technology (IUT), Isfahan. Further partial financial support of Iran Nanotechnology Initiative Council (INIC), National Elite Foundation (NEF), and Center of Excellence in Sensors and Green Chemistry (IUT) is also gratefully acknowledged.

References

1. Jeon IY, Baek JB (2010) Nanocomposites derived from polymers and inorganic nanoparticles. Materials 3:3654–3674
2. Paul DR, Robeson LM (2008) Polymer nanotechnology: nanocomposites. Polymer 49:3187–3204
3. Jetson R, Yin K, Donovan K, Zhu Z (2010) Polymer-supported nanocomposites for environmental application: a review. Mater Chem Phys 124:417–421
4. Zhang Q, Chou TP, Russo B, Jenekhe SA, Cao G (2008) Polydisperse aggregates of ZnO nanocrystallites: a method for energy-conversion-efficiency enhancement in dye-sensitized solar cells. Adv Funct Mater 18:1654–1660
5. Moezzi A, McDonagh AM, Cortie MB (2012) Review: zinc oxide particles: synthesis, properties and applications. Chem Eng J 185–186:1–22
6. Tu YF, Fu QM, Sang JP, Zou XW (2012) Synthesis and photoluminescence properties of the ZnO@SnO_2 core–shell nanorod arrays. J Mater Sci 47:1541–1545. doi:10.1007/s10853-011-5944-3
7. Ma C, Zhou Z, Wei H, Yang Z, Wang Z, Zhang Y (2011) Rapid large-scale preparation of ZnO nanowires for photocatalytic application. Nanoscale Res Lett 6:536–540
8. Lv J, Gong W, Huang K, Zhu J, Meng F, Song X, Sun Z (2011) Effect of annealing temperature on photocatalytic activity of ZnO thin films prepared by sol–gel method. Superlattices Microstruct 50:98–106
9. Du QG, Alagappan G, Dai H, Demir HV, Yu HY, Sun XW, Kam CH (2012) UV-blocking ZnO nanostructure anti-reflective coatings. Opt Commun 285:3238–3241
10. Chen Q, Sun Y, Wang Y, Cheng H, Wang QM (2013) ZnO nanowires–polyimide nanocomposite piezoresistive strain sensor. Sens Actuators A 190:161–167
11. Qiu Y, Yang M, Fan H, Xu Y, Shao Y, Yang X, Yang S (2014) Synthesis of ZnO nanorod arrays on Zn substrates by a gas–solution–solid method and their application as an ammonia sensor. J Mater Sci 49:347–352. doi:10.1007/s10853-013-7711-0
12. Abdolmaleki A, Mallakpour S, Borandeh S (2012) The use of novel biodegradable, optically active and nanostructured poly(amide-ester-imide) as a polymer matrix for preparation of modified ZnO based bionanocomposites. Mater Res Bull 47:1123–1129
13. Fan X, Qin X, Jing L, Luan Y, Xie M (2012) Controllable synthesis of floatable nanocrystalline Ag2S and Ag by a silane coupling agent-modified solvothermal method. Mater Res Bull 47:3732–3737
14. Joni IM, Balgis R, Ogi T, Iwaki T, Okuyama K (2011) Surface functionalization for dispersing and stabilizing hexagonal boron nitride nanoparticle by bead milling. Colloids Surf A 388:49–58
15. Hsiao SH, Liou GS, Kung YC, Lee YJ (2010) Synthesis and characterization of electrochromic poly(amide–imide)s based on the diimide-diacid from 4,4′-diamino-4″-methoxytriphenylamine and trimellitic anhydride. Eur Polym J 46:1355–1366
16. Mallakpour S, Banihassan K, Sabzalian MR (2013) Novel bioactive chiral poly(amide–imide)s containing different amino acids linkages: studies on synthesis, characterization and biodegradability. J Polym Environ 21:568–574
17. Rajesh S, Maheswari P, Senthilkumar S, Jayalakshmi A, Mohan D (2011) Preparation and characterisation of poly(amide–imide) incorporated cellulose acetate membranes for polymer enhanced ultrafiltration of metal ions. Chem Eng J 171:33–44
18. Lin HL, Chang HL, Juang TY, Lee RH, Dai SA, Liu YL, Jeng RJ (2009) Nonlinear optical, poly(amide–imide)–clay nanocomposites comprising an azobenzene moiety synthesised via sequential self-repetitive reaction. Dyes Pigments 82:76–83
19. Mallakpour S, Dinari M (2011) Insertion of novel optically active poly(amide–imide) chains containing pyromellitoyl-bis-L-phenylalanine linkages into the nanolayered silicates modified with L-tyrosine through solution intercalation. Polymer 52:2514–2523
20. Mallakpour S, Zadehnazari A (2013) The production of functionalized multiwall carbon nanotube/amino acid-based poly(amide–imide) composites containing a pendant dopamine moiety. Carbon 56:27–37
21. Ma X, Lee NH, Oh HJ, Hwang JS, Kim SJ (2010) Preparation and characterization of silica/polyamide–imide nanocomposite thin films. Nanoscale Res Lett 5:1846–1851
22. Mallakpour S, Zadehnazari A (2012) Novel optically active poly(amide-thioester-imide)s containing L-α-amino acids and thiadiazol anticorrosion group: production and characterization. High Perform Polym 25:377–386
23. Mallakpour S, Soltanian S (2012) Synthesis and structural characterization of novel chiral nanostructured poly(esterimide)s containing different natural amino acids and 4,4′-thiobis(2-tert-butyl-5-methylphenol) linkages. J Appl Polym Sci 124:5089–5096
24. Mallakpour S, Zadehnazari A (2011) Advances in synthetic optically active condensation polymers—a review. Express Polym Lett 5:142–181
25. Mallakpour S, Dehghani M, Sabzalian MR (2013) Green step-grow polymerization of biodegradable amino acid based diacids with 3,5-diamino-*N*-(thiazole-2-yl)benzamide: characterization and study on bioactivity. J Polym Res 20:85–90
26. Mallakpour SE, Hajipour AR, Roohipour-fard R (2000) Direct polycondensation of *N*-trimellitylimido-L-leucine with aromatic diamines. Eur Polym J 36:2455–2462